PRECONDITIONERS FOR VARIABLE-COEFFICIENT FINITE-VOLUME STOKES SOLVERS

M. CAI, A. NONAKA, B. E. GRIFFITH, J. B. BELL, A. DONEV

Abstract. We develop several robust preconditioners for solving the saddle-point linear systems that arise ~~upon~~ from spatial discretization of unsteady and steady variable-coefficient Stokes equations on a uniform staggered grid. Building on the success of using the classical projection method as a preconditioner for the coupled velocity-pressure system [*B. Griffith, J. Comp. Phys., 228 (2009), pp. 7565–7595*], as well as established techniques for steady Stokes flow in the finite-element literature, we construct preconditioners that employ separate Helmholtz or Poisson solvers for the pressure and the velocity subproblems. We find that a single cycle of a standard geometric multigrid can be used as inexact solvers for these subproblems. Contrary to traditional wisdom, we find that the overall cost of solving the Stokes system is comparable to the cost of classical projection or fractional step methods for incompressible flow, even for steady flow and in the presence of large density and viscosity contrast. Two of the five preconditioners considered here are found to be robust to GMRES restarts and to increasing problem size, making them suitable for large-scale problems. Our work opens many possibilities for constructing novel unsplit implicit temporal integrators for finite-volume spatial discretizations of low Mach and incompressible flow problems.

– preconditioners

~~[illegible]~~ different type of alg. ~~[illegible]~~ Don't want implicit advection

Keywords Stokes flow; variable density; variable viscosity; saddle point problems; projection method; preconditioning; GMRES.

1. Introduction. Many numerical methods for solving the time-dependent (unsteady) incompressible [3, 2, 18, 16] or low Mach number [33, 10] equations require the solution of a linear unsteady Stokes flow subproblem. The linear steady Stokes problem is of particular interest for low Reynolds number flows [30, 17]. In this work, we develop efficient linear solvers for the unsteady and steady Stokes equations in the presence of variable density and viscosity. Specifically, we consider the coupled velocity-pressure Stokes system [39, 15]

issues for boundary layers

$$\left\{ \begin{array}{l} \rho \boldsymbol{u}_t + \boldsymbol{\nabla} p = \boldsymbol{\nabla} \cdot \boldsymbol{\tau}(\boldsymbol{u}) + \boldsymbol{f}, \\ \boldsymbol{\nabla} \cdot \boldsymbol{u} = g, \end{array} \right. \tag{1.1}$$

$\rho u_t \sim (\rho u)_t$

should be a compatibility condition for pure Dirichlet BC.

where $\rho(\boldsymbol{r},t)$ is the (potentially variable) density, $\boldsymbol{u}(\boldsymbol{r},t)$ is the velocity, $p(\boldsymbol{r},t)$ is the pressure, $\boldsymbol{f}(\boldsymbol{r},t)$ is a force density, and $\boldsymbol{\tau}(\boldsymbol{u})$ is the viscous stress tensor. A nonzero velocity-divergence $g(\boldsymbol{r},t)$ arises, for example, in low Mach number models because of compositional or temperature variations [33]. The viscous stress $\boldsymbol{\tau}(\boldsymbol{u})$ is $\mu \boldsymbol{\nabla} \boldsymbol{u}$ for constant viscosity incompressible flow, $\mu \left[\boldsymbol{\nabla} \boldsymbol{u} + (\boldsymbol{\nabla} \boldsymbol{u})^T \right]$ when $g = 0$ (incompressible flow), and $\mu \left[\boldsymbol{\nabla} \boldsymbol{u} + (\boldsymbol{\nabla} \boldsymbol{u})^T \right] + (\gamma - \frac{2}{3}\mu)(\boldsymbol{\nabla} \cdot \boldsymbol{u})\boldsymbol{I}$ when $g \neq 0$, where $\mu(\boldsymbol{r},t)$ is the (potentially variable) shear viscosity and $\gamma(\boldsymbol{r},t)$ is the (potentially variable) bulk viscosity. When the inertial term is neglected, $\rho \boldsymbol{u}_t = 0$, (1.1) is reduced to the time-independent (steady-state) Stokes equations. In this work we consider periodic boundary conditions and physical boundary conditions that involve velocity only, notably no-slip and free-slip physical boundaries.

Spatial discretization of (1.1) can be carried out using standard finite-volume or finite-element techniques. Applying the backward Euler scheme to solve the spatially-discretized equations with time step size Δt, gives the following discrete system for the velocity $\boldsymbol{u}^{n+1}$ and the pressure p^{n+1} at the end of time step n,

$$\left\{ \begin{array}{l} \rho \left(\frac{\boldsymbol{u}^{n+1} - \boldsymbol{u}^n}{\Delta t} \right) + \boldsymbol{\nabla} p^{n+1} = \boldsymbol{\nabla} \cdot \boldsymbol{\tau}\left(\boldsymbol{u}^{n+1}\right) + \boldsymbol{f}^{n+1}, \\ \boldsymbol{\nabla} \cdot \boldsymbol{u}^{n+1} = g^{n+1}, \end{array} \right. \tag{1.2}$$

where $\boldsymbol{f}^{n+1}$ contains external forcing terms such as gravity and any explicitly-handled terms such as, for example, advection. Similar linear systems are obtained with other implicit and semi-implicit temporal discretizations [3, 2, 18]. In the limit $\rho/\Delta t \to 0$, the system (1.2) reduces to the steady Stokes equations. Here we will assume that the spatial discretization is stable, more precisely, that the Stokes system (1.2) is "uniformly" solvable as the spatial discretization becomes finer. This means that a suitable measure of the conditioning number of (1.2) remains bounded as the grid spacing $h \to 0$. In the context of finite-element methods, this is equivalent to the well-known inf − sup or Ladyženskaja-Babuška-Brezzi (LBB) condition. Here we employ the classical staggered-grid [23] discretization on a uniform grid, which is known to be a stable discretization [38, 31]. We expect that the preconditioners

Analog to lowest order Raviart – Thomas space developed here can be relatively straightforwardly generalized to other stable spatial discretizations, such as finite-element techniques [39, 15] or recently-developed adaptive mesh staggered schemes [19, 17]. Note, however, that collocated finite-volume discretizations of the Navier-Stokes equations do not provide a stable discretization, motivating the development of approximate-projection methods [1].

There ~~is~~ are significant differences in the treatment of (1.2) in the finite-volume and finite-element literature. In the finite-element literature, there is a long history of numerical methods for solving the Stokes equations, especially in the time-independent (steady) context [39, 15]. By contrast, in the context of high-resolution finite-volume methods, the dominant paradigm has been to use a splitting (fractional-step) or projection method [9, 7] to separate the pressure and velocity updates. In part, this choice has been motivated by the target applications, which are often high Reynolds number, or even inviscid flows. In the inviscid limit, the splitting error vanishes, and for sufficiently large Reynolds number flows the time step size dictated by advective stability constraints makes the splitting error relatively small. At the same time, the preference for splitting methods stems, in large part, from the perception that solving the saddle-point problem (1.2) is much more difficult than solving the pressure and velocity subproblems; to quote the authors of Ref. [7], "Spatially discretized versions of the coupled Eqs. ... are cumbersome to solve directly." In fact, one of the first second-order projection methods [3] was developed by starting with a Crank-Nicolson variant of (1.2) and then trying to approximate it using pressure-velocity splitting due to the perceived difficulty in solving the coupled system.

Fractional-step approaches, however, suffer from several significant shortcomings. It is well-known, for example, that the splitting introduces a commutator error that leads to the appearance of "spurious" or "parasitic" modes [11, 7] in the presence of physical boundaries. Furthermore, the imposition of boundary conditions that couple pressure and velocity is difficult and requires the creation of artificial intermediate boundary conditions. Lastly, the splitting error becomes larger as viscous effects become more dominant, and projection methods do not apply in the steady Stokes regime. Recognizing these problems, one of us investigated the use of projection-like methods as preconditioners for a Krylov method for solving the coupled system (1.2) [18]. It was found that, contrary to traditional wisdom, the saddle-point problem (1.2) can be efficiently solved using standard multigrid techniques for the velocity and pressure subproblems, for a broad range of parameters. Here we improve and generalize the preconditioners developed in Ref. [18] to account for variable density and variable viscosity, as well as to robustly handle very small or zero (steady) Reynolds number flows. We also investigate several alternative preconditioners that solve the velocity and pressure subproblems in different orders. Several of these methods have already been proposed and studied in the finite-element literature [4, 5, 14, 15, 13, ?, 24, 25, 26, 27, 28, 30, 29, 39]. However, most works are aimed at solving constant density and constant viscosity problems, or are restricted to the steady case. We ?
See ~~will not~~ attempt to review the extensive finite-element literature on preconditioners for Stokes flow here [15]; instead, we will point out the similarities and differences with prior work for each of the preconditioners that we study. In the finite-volume context, the work most closely related to our work is Ref. [16], which focuses on steady Stokes flow in the presence of large viscosity contrast (jumps) for geodynamic applications. Notably, both our work and the work presented in Ref. [16] are based on a staggered finite-volume fluid solver and geometric multigrid solvers.

The preconditioners that we investigate are built using two crucial subsolvers. The first of these is a linear solver for the inviscid problem

$$\left\{\begin{array}{l}\rho\left(\frac{\boldsymbol{u}^{n+1}-\boldsymbol{u}^{n}}{\Delta t}\right)+\boldsymbol{\nabla}p^{n+1}=\boldsymbol{f}^{n+1},\\ \boldsymbol{\nabla}\cdot\boldsymbol{u}^{n+1}=g^{n+1},\end{array}\right. \tag{1.3}$$

the solution of which requires solving a density-weighted pressure Poisson equation

$$-\boldsymbol{\nabla}\cdot\left(\rho^{-1}\boldsymbol{\nabla}p^{n+1}\right)=g^{n+1}-\boldsymbol{\nabla}\cdot\left(\boldsymbol{u}^{n+1}+\rho^{-1}\boldsymbol{f}^{n+1}\Delta t\right).$$

For the staggered-grid finite-volume discretization we employ here, this Poisson problem can efficiently be solved using standard geometric multigrid techniques [2]. The second subsolver required by the preconditioners is a linear solver for the unconstrained variable-coefficient velocity equation,

$$\rho\left(\frac{\boldsymbol{u}^{n+1}-\boldsymbol{u}^{n}}{\Delta t}\right)=\boldsymbol{\nabla}\cdot\boldsymbol{\tau}\left(\boldsymbol{u}^{n+1}\right)+\boldsymbol{f}^{n+1}. \tag{1.4}$$

Note that both (1.3) or (1.4) use the same boundary conditions for velocity as the coupled problem, and that no boundary conditions are required for the pressure when solving (1.3) on a staggered grid. For constant viscosity incompressible flow $\boldsymbol{\nabla}\cdot\boldsymbol{\tau}(\boldsymbol{u})=\mu\boldsymbol{\nabla}^2\boldsymbol{u}$ and therefore (1.4) is a system of d uncoupled Helmholtz equations, where d is the dimensionality. These can be solved efficiently using standard geometric multigrid techniques. For variable viscosity flows the different components of velocity are coupled. Here we develop an effective geometric multigrid method for solving (1.4) based on the classical red-black coloring smoother for the scalar Poisson equation. Since the solution of either (1.3) or (1.4) is itself a costly iterative process, it is crucial that the preconditioners require only approximate subsolvers. More precisely, preconditioning should only require the application of linear operators that are spectrally-equivalent [15] to the exact solution operators for (1.3) or (1.4). Here we use one or a few cycles of geometric multigrid as approximate subsolvers.

Our goal will be to optimize the various parameters and thus give specific prescriptions that practitioners can use with minimal effort. More importantly, we will strive to construct solvers for the Stokes system that are (nearly) as computationally efficient as traditional fractional step or split methods, and use traditional building blocks available in many existing codes. We will also aim to construct preconditioners that can easily be generalized to other situations and spatial discretizations by simply constructing approximate solvers for (1.3) and (1.4). For example, boundary conditions that couple pressure and viscous stress can be handled by imposing approximate boundary conditions for the subsolvers. In Ref. [18], at physical boundaries on which prescribed normal tractions (normal components of the stress tensor) are imposed, Neumann conditions are imposed on the normal velocity component when solving (1.4) and Dirichlet conditions are imposed for the pressure when solving (1.3). For adaptively-refined meshes [19, 17], multilevel geometric multigrid techniques can be used to solve the pressure and velocity subproblems [2, 19].

The organization of this paper is as follows. In section 2, we introduce several preconditioners based on approximating the inverse of the Schur complement. At first we keep the presentation rather general in order to facilitate future generalizations, and then in Section 3 we specialize to a particular staggered-grid second-order finite-volume discretization and give details of our numerical implementation. In Section 4 we perform a detailed study of the efficiency and robustness of the various preconditioners, and select the optimal values for several algorithmic parameters. Finally, we offer some conclusions in Section 5, and then give several technical derivations in an extensive Appendix.

2. Preconditioners. In this section we construct several preconditioners for solving the saddle-point linear system (1.2) that arises after spatio-temporal discretization of (1.1). For increased generality, we write this system in the form,

$$\boldsymbol{M}\begin{pmatrix}\boldsymbol{x}_u\\ \boldsymbol{x}_p\end{pmatrix}=\begin{pmatrix}\boldsymbol{A} & \boldsymbol{G}\\ -\boldsymbol{D} & \boldsymbol{0}\end{pmatrix}\begin{pmatrix}\boldsymbol{x}_u\\ \boldsymbol{x}_p\end{pmatrix}=\begin{pmatrix}\boldsymbol{b}_u\\ \boldsymbol{b}_p\end{pmatrix}, \tag{2.1}$$

where $(\boldsymbol{x}_u,\,\boldsymbol{x}_p)^T$ denote the velocity and pressure degrees of freedom, $(\boldsymbol{b}_u,\,\boldsymbol{b}_p)^T$ are the velocity and pressure right hand sides, $\boldsymbol{D}$ denotes a discrete divergence operator, and $\boldsymbol{G}$ is a discrete gradient operator. Note that for the staggered-grid discretization that we describe in Section 3 the gradient and divergence operators are duals for periodic or no-slip boundary conditions, $\boldsymbol{G}=(-\boldsymbol{D})^{\star}$, where star denotes adjoint, making $\boldsymbol{M}=\boldsymbol{M}^{\star}$ a self-adjoint matrix. Here the linear velocity operator $\boldsymbol{A}=\theta\boldsymbol{\rho}-\boldsymbol{L}_{\mu}$ combines inertial and viscous effects, where θ is a parameter that is zero for steady Stokes flow, and $\theta\sim\Delta t^{-1}$ for unsteady flow. The operator $\boldsymbol{\rho}$ is a density (mass) matrix, such that $\boldsymbol{\rho}\boldsymbol{x}_u$ is a spatially-discrete (conserved) momentum field. The viscous operator is denoted with $\boldsymbol{L}_{\mu}$, with $\boldsymbol{L}_{\mu}\boldsymbol{u}$ being a spatial discretization of $\boldsymbol{\nabla}\cdot\boldsymbol{\tau}(\boldsymbol{u})$.

The saddle-point problem (2.1) can formally be solved by using the inverse of the Schur complement,

$$\boldsymbol{S}^{-1} = \left(-\boldsymbol{D}\boldsymbol{A}^{-1}\boldsymbol{G}\right)^{-1},$$

to obtain the exact solution for the pressure,

$$\boldsymbol{x}_p = -\boldsymbol{S}^{-1}(\boldsymbol{D}\boldsymbol{A}^{-1}\boldsymbol{b}_u + \boldsymbol{b}_p), \tag{2.2}$$

and for the velocity degrees of freedom,

$$\boldsymbol{x}_u = \boldsymbol{A}^{-1}(\boldsymbol{b}_u - \boldsymbol{G}\boldsymbol{x}_p) = \boldsymbol{A}^{-1}\boldsymbol{b}_u + \boldsymbol{A}^{-1}\boldsymbol{G}\boldsymbol{S}^{-1}(\boldsymbol{D}\boldsymbol{A}^{-1}\boldsymbol{b}_u + \boldsymbol{b}_p). \tag{2.3}$$

These formal solutions are not useful in practice because the Schur complement cannot even be formed explicitly for large three-dimensional grids, yet alone inverted efficiently. In Ref. [16], the authors investigate evaluating the action of $\boldsymbol{S}^{-1}$ in (2.2) by an outer Krylov solver, which itself relies on evaluating the action of $\boldsymbol{A}^{-1}$ in an inner (nested) Krylov solver. We do not investigate this approach here and instead focus on what the authors of Ref. [16] call the "fully coupled preconditioned approach", in which an approximation of the Schur complement solution is used to construct an effective preconditioner for a Krylov solver applied to the saddle-point problem (2.1). The key part in designing preconditioners for (2.1) is approximating the (inverse of the) Schur complement, specifically, constructing an operator $\mathcal{S}^{-1}$ that is spectrally-equivalent to $\boldsymbol{S}^{-1}$ [14].

too close a font.

In order to motivate the approximation of $\boldsymbol{S}^{-1}$ used in Ref. [18], let us consider the case of constant viscosity μ_0 and constant density ρ_0. In this case $\boldsymbol{A} = \theta\rho_0\boldsymbol{I} - \mu_0\boldsymbol{L}$, where $\boldsymbol{I}$ denotes an identity matrix of the appropriate size and $\boldsymbol{L}$ is a discrete vector Laplacian operator, constructed taking into account the imposed velocity boundary conditions. We then have

try different math font

$$\boldsymbol{S}^{-1} = \left[-\boldsymbol{D}\left(\theta\rho_0\boldsymbol{I} - \mu_0\boldsymbol{L}\right)^{-1}\boldsymbol{G}\right]^{-1} \approx \left[\left(-\boldsymbol{D}\boldsymbol{G}\right)\left(\theta\rho_0\boldsymbol{I} - \mu_0\boldsymbol{L}_p\right)^{-1}\right]^{-1} = -\theta\rho_0\boldsymbol{L}_p^{-1} + \mu_0\boldsymbol{I} \tag{2.4}$$

where $\boldsymbol{L}_p = \boldsymbol{D}\boldsymbol{G}$ denotes a scalar (pressure) discrete Laplacian operator, and have assumed the commuting property $\boldsymbol{L}\boldsymbol{G} \approx \boldsymbol{G}\boldsymbol{L}_p$, which is an exact identity for the staggered grid discretization ~~for~~ periodic systems. applied to

Here we generalize (2.4) to variable density and viscosity through a simple construction. The basic idea is that the first part of the Schur complement approximation, $\theta\rho_0\boldsymbol{L}_p^{-1}$, corresponds to the inviscid limit. For variable density, this term should become $\theta\boldsymbol{L}_\rho^{-1}$, where

Early ref. is Bell-Marcus

$$\boldsymbol{L}_\rho = \boldsymbol{D}\rho^{-1}\boldsymbol{G}$$

is a discretization of the density-weighted Poisson operator $\boldsymbol{\nabla}\cdot\rho^{-1}\boldsymbol{\nabla}$ that also appears in traditional variable-density projection methods [2]. Therefore, for variable-density constant-viscosity flow, $\boldsymbol{\nabla}\cdot\boldsymbol{\tau} = \mu_0\boldsymbol{\nabla}^2\boldsymbol{u}$, we employ the approximation [18]

$$\boldsymbol{S}^{-1} \approx \mathcal{S}^{-1} = -\theta\boldsymbol{L}_\rho^{-1} + \mu_0\boldsymbol{I}. \tag{2.5}$$

The term $\mu_0\boldsymbol{I}$ in (2.4) is an analogue of the viscous operator $\boldsymbol{L}_\mu$ that acts not on velocity degrees of freedom but rather on pressure degrees of freedom. This has to be constructed on a case-by-case basis, and in the constant viscosity setting it corresponds to the viscous pressure-correction term proposed by Brown, Cortez and Minion [7] in the context of second-order projection methods. For incompressible flow, $\boldsymbol{\tau}(\boldsymbol{u}) = \mu\left[\boldsymbol{\nabla}\boldsymbol{u} + (\boldsymbol{\nabla}\boldsymbol{u})^T\right]$, the Fourier-space calculation described in Appendix A suggests replacing the term $\mu_0\boldsymbol{I}$ with $2\boldsymbol{\mu}$, where $\boldsymbol{\mu}$ a diagonal matrix of viscosities corresponding to each pressure degree of freedom [**Donev: In the more general setting, perhaps some weighting will be needed for the viscosities?**]. This gives the Schur complement inverse approximation

$$\boldsymbol{S}^{-1} \approx \mathcal{S}^{-1} = -\theta\boldsymbol{L}_\rho^{-1} + 2\boldsymbol{\mu}, \tag{2.6}$$

which is called the "local viscosity" preconditioner in Ref. [16]. Note however that the prefactor of two in front of the viscosity matrix is not included in Eq. (36) in Ref. [16], as suggested by our analysis of the constant-viscosity problem in Appendix A. When bulk viscosity is included, $\boldsymbol{\tau}(\boldsymbol{u}) = \mu\left[\boldsymbol{\nabla}\boldsymbol{u} + (\boldsymbol{\nabla}\boldsymbol{u})^T\right] + (\gamma - \frac{2}{3}\mu(\boldsymbol{\nabla}\cdot\boldsymbol{u}))\boldsymbol{I}$, we take

$$\boldsymbol{S}^{-1} \approx \widetilde{\boldsymbol{S}}^{-1} = -\theta \boldsymbol{L}_\rho^{-1} + \left(\boldsymbol{\gamma} + \frac{4}{3}\boldsymbol{\mu}\right), \tag{2.7}$$

where $\boldsymbol{\gamma}$ is the diagonal matrix of bulk viscosities. As we demonstrate in Appendix A, these approximations are exact for periodic systems if the density and viscosity are constant. In all other cases they are approximations that are expected to be good in regions far from boundaries where the coefficients do not vary significantly. Our numerical experiments support this intuition.

It is important to observe that the pressure-space viscous operator in (2.6) does not make use of the velocity boundary conditions, unlike the velocity-space viscous operator $\boldsymbol{L}_\mu$. We have investigated the alternative approximations

$$\boldsymbol{S}^{-1} \approx -\theta \boldsymbol{L}_\rho^{-1} - \boldsymbol{L}_\rho^{-1}\boldsymbol{D}\boldsymbol{\rho}^{-1}\boldsymbol{L}_\mu\boldsymbol{\rho}^{-1}\boldsymbol{G}\boldsymbol{L}_\rho^{-1},$$

as well as

B t

$$\boldsymbol{S}^{-1} \approx -\theta \boldsymbol{L}_\rho^{-1} - \boldsymbol{L}_p^{-1}\left(\boldsymbol{D}\boldsymbol{L}_\mu\boldsymbol{G}\right)\boldsymbol{L}_p^{-1},$$

which is similar to the BFBt preconditioner of Elman [14] in the steady-state case, and is also investigated in Ref. [16]. These approximations do utilize the velocity boundary conditions since they involve the viscous operator $\boldsymbol{L}_\mu$. We have, however, not found the increased computational cost of these more elaborate approximations to the Schur complement inverse to be justified in terms of the overall performance of the Stokes solver.

2.1. Projection Preconditioner. In the first preconditioner we consider, which we ~~will call~~ denote with $\boldsymbol{P}_1$, we use one step of the classical projection method (fractional step algorithm) [9, 3, 18] as a preconditioner. In $\boldsymbol{P}_1$, we use (2.2) to estimate the pressure, and make a commuting assumption in (2.3),

$$\boldsymbol{A}^{-1}\boldsymbol{G}\boldsymbol{S}^{-1} = \boldsymbol{A}^{-1}\boldsymbol{G}(-\boldsymbol{D}\boldsymbol{A}^{-1}\boldsymbol{G})^{-1} \approx -\boldsymbol{A}^{-1}\boldsymbol{A}\boldsymbol{\rho}^{-1}\boldsymbol{G}\boldsymbol{L}_\rho^{-1} = -\boldsymbol{\rho}^{-1}\boldsymbol{G}\boldsymbol{L}_\rho^{-1},$$

which gives the velocity estimate

$$\boldsymbol{x_u} \approx \boldsymbol{A}^{-1}\boldsymbol{b_u} - \boldsymbol{\rho}^{-1}\boldsymbol{G}\boldsymbol{L}_\rho^{-1}(\boldsymbol{D}\boldsymbol{A}^{-1}\boldsymbol{b_u} + \boldsymbol{b}_p). \tag{2.8}$$

Note that this velocity estimate (2.8) satisfies the divergence condition exactly, $\boldsymbol{D}\boldsymbol{x_u} = -\boldsymbol{b}_p$, more precisely, $\boldsymbol{x_u}$ is the L_2 projection of the unconstrained velocity estimate $\boldsymbol{A}^{-1}\boldsymbol{b_u}$ onto the divergence constraint. ?

In practical implementation, the exact subproblem solvers need to be replaced by approximat~~e~~ions. ~~subproblem solves~~. Specifically, $\boldsymbol{A}^{-1}$ is approximated by the inexact velocity solver $\widetilde{\boldsymbol{A}}^{-1}$, $\boldsymbol{L}_\rho^{-1}$ is approximate ? ~~implemented by the inexact~~ pressure Poisson solver $\widetilde{\boldsymbol{L}}_\rho^{-1}$, and $\boldsymbol{S}^{-1}$ is replaced by $\widetilde{\mathcal{S}}^{-1}$, an inexact solver for the approximate Schur complement inverse $\widetilde{\mathcal{S}}^{-1}$ given by (2.6) for incompressible flow. In summary, for the variable-coefficient Stokes problem, the projection preconditioner $\boldsymbol{P}_1$ is defined by the block factorization

$$\boldsymbol{P}_1^{-1} = \begin{pmatrix} \boldsymbol{I} & \boldsymbol{\rho}^{-1}\boldsymbol{G}\widetilde{\boldsymbol{L}}_\rho^{-1} \\ 0 & \widetilde{\mathcal{S}}^{-1} \end{pmatrix} \begin{pmatrix} \boldsymbol{I} & 0 \\ -\boldsymbol{D} & -\boldsymbol{I} \end{pmatrix} \begin{pmatrix} \widetilde{\boldsymbol{A}}^{-1} & 0 \\ 0 & \boldsymbol{I} \end{pmatrix}. \tag{2.9}$$

This factorization clearly shows the three main steps in the application of the preconditioner. First~~ly~~, a velocity subproblem is solved inexactly (right-most block). Second~~ly~~, $\boldsymbol{b}_c = \boldsymbol{D}\widetilde{\boldsymbol{A}}^{-1}\boldsymbol{b_u} + \boldsymbol{b}_p$ is computed (middle block). Third~~ly~~, a Poisson problem is solved approximately to compute $\widetilde{\boldsymbol{L}}_\rho^{-1}\boldsymbol{b}_c$ and, lastly, the pressure and velocity estimates are computed (first block). For constant-coefficient periodic problems with exact subsolvers, the projection preconditioner is an exact solver for the coupled Stokes equations since both (2.4) and (2.8) are exact.

For the constant viscosity and density Stokes problem, a projection preconditioner very similar to $\boldsymbol{P}_1$ was first proposed by one of us in Ref. [18]. In this work we generalize the projection preconditioner to the case of variable viscosity and density. Even in the constant-coefficient case, there is a small but important difference between $\boldsymbol{P}_1$ and the previous projection preconditioner in Ref. [18], which uses the following approximation of the Schur complement inverse,

$$\boldsymbol{S}^{-1} \approx \widetilde{\boldsymbol{S}}^{-1} = -\left(\theta\rho_0 \boldsymbol{I} - \mu_0 \boldsymbol{L}_p\right) \widetilde{\boldsymbol{L}}_p^{-1},$$

rather than the approximation (2.5) used here , $\widetilde{\boldsymbol{S}}^{-1} = -\theta\rho_0 \widetilde{\boldsymbol{L}}_p^{-1} + \mu_0 \boldsymbol{I}$, which we have found to give a more efficient solver overall. The two approximations are identical when ~~an~~ exact Poisson solvers are used, $\widetilde{\boldsymbol{L}}_p^{-1} = \boldsymbol{L}_p^{-1}$, but not when an approximate solver is employed.

2.2. Lower Triangular Preconditioner. For our second preconditioner, which we denote with $\boldsymbol{P}_2$, we use (2.2) for the pressure estimate, but the velocity estimate takes the simpler form

$$\boldsymbol{x}_{\boldsymbol{u}} \approx \boldsymbol{A}^{-1} \boldsymbol{b}_{\boldsymbol{u}}, \tag{2.10}$$

obtained by discarding the second part in (2.3). If we further approximate the matrix inverses with inexact solves, namely, replacing $\boldsymbol{A}^{-1}$ by $\widetilde{\boldsymbol{A}}^{-1}$, $\boldsymbol{L}_\rho^{-1}$ by $\widetilde{\boldsymbol{L}}_\rho^{-1}$, and $\boldsymbol{S}^{-1}$ by $\widetilde{\boldsymbol{S}}^{-1}$, the second preconditioner is given by the block factorization

$$\boldsymbol{P}_2^{-1} = \begin{pmatrix} \boldsymbol{I} & 0 \\ 0 & -\widetilde{\boldsymbol{S}}^{-1} \end{pmatrix} \begin{pmatrix} \boldsymbol{I} & 0 \\ \boldsymbol{D} & \boldsymbol{I} \end{pmatrix} \begin{pmatrix} \widetilde{\boldsymbol{A}}^{-1} & 0 \\ 0 & \boldsymbol{I} \end{pmatrix}. \tag{2.11}$$

By combing all the terms in the right hand side of (2.11), we see that $\boldsymbol{P}_2$ is actually an approximation of the inverse of the lower triangular preconditioner previously studied by several other groups [8, 24, 25, 26, 27],

$$\boldsymbol{P}_2^{-1} \approx \begin{pmatrix} \boldsymbol{A} & 0 \\ -\boldsymbol{D} & -\boldsymbol{S} \end{pmatrix}^{-1}. \tag{2.12}$$

Notice that for steady Stokes flow, $\theta = 0$, the application of $\boldsymbol{P}_2^{-1}$ does not require any pressure Poisson solvers, unlike the projection preconditioner. Therefore, a single application of $\boldsymbol{P}_2^{-1}$ can be significantly less expensive computationally than an application of $\boldsymbol{P}_1^{-1}$. For unsteady flows $\boldsymbol{P}_1$ and $\boldsymbol{P}_2$ involve nearly the same operations and applying them has similar computational cost.

2.3. Upper Triangular Preconditioner. Alternatively, one can assume $\boldsymbol{D}\boldsymbol{A}^{-1}\boldsymbol{b}_{\boldsymbol{u}} \approx 0$ to obtain $\boldsymbol{x}_p = -\boldsymbol{S}^{-1}\boldsymbol{b}_p$ and

$$\boldsymbol{x}_{\boldsymbol{u}} = \boldsymbol{A}^{-1}(\boldsymbol{b}_{\boldsymbol{u}} + \boldsymbol{G}\boldsymbol{S}^{-1}\boldsymbol{b}_p).$$

Replacing the exact solvers with inexact solvers, we obtain our third preconditioner in block factorization form,

$$\boldsymbol{P}_3^{-1} = \begin{pmatrix} \widetilde{\boldsymbol{A}}^{-1} & 0 \\ 0 & \boldsymbol{I} \end{pmatrix} \begin{pmatrix} \boldsymbol{I} & -\boldsymbol{G} \\ 0 & \boldsymbol{I} \end{pmatrix} \begin{pmatrix} \boldsymbol{I} & 0 \\ 0 & -\widetilde{\boldsymbol{S}}^{-1} \end{pmatrix}, \tag{2.13}$$

which ~~and~~ is exactly the same as the "fully coupled" approach with the "local viscosity" preconditioner studied in Ref. [16], generalized here to time-dependent problems. If we combine all the terms in the right hand side of (2.13), then we see that $\boldsymbol{P}_3$ is actually an approximation of the inverse of the upper triangular preconditioner [8, 24, 25, 26, 27],

$$\boldsymbol{P}_3^{-1} \approx \begin{pmatrix} \boldsymbol{A} & \boldsymbol{G} \\ 0 & -\boldsymbol{S} \end{pmatrix}^{-1}. \tag{2.14}$$

The computational cost of applying $\boldsymbol{P}_3^{-1}$ is very similar to that of applying $\boldsymbol{P}_2^{-1}$.

2.4. Other preconditioners. In addition to the three main preconditioners (projection, lower and upper triangular) we study here, we have investigated some other preconditioners. The simplest Schur-complement based preconditioner one can construct is the block diagonal preconditioner [8, 25, 26, 27]

$$\boldsymbol{P}_4^{-1} = \begin{pmatrix} \widetilde{\boldsymbol{A}}^{-1} & \boldsymbol{0} \\ \boldsymbol{0} & -\widetilde{\mathcal{S}}^{-1} \end{pmatrix}. \tag{2.15}$$

This preconditioner has the lowest computational cost of all the preconditioners but also makes the poorest approximation to the exact solution (2.2,2.3). In the appendix, we show that $\boldsymbol{P}_1$, $\boldsymbol{P}_2$, $\boldsymbol{P}_3$ all give the same spectrum for the preconditioned linear operator. It is also well-known that $\boldsymbol{P}_1$, $\boldsymbol{P}_2$, $\boldsymbol{P}_3$, and $\boldsymbol{P}_4$ are all spectrally-equivalent if exact solvers are used [15].

As an alternative approximation to (2.2,2.3) that is more accurate than the previous approximations, we consider a fifth preconditioner, denoted by $\boldsymbol{P}_5$. The action of the inverse of this preconditioner $\boldsymbol{P}_5^{-1}$ cannot easily be written in block-factorization form so we present in the form of pseudo-code:

1. Solve for $\boldsymbol{x}_{\boldsymbol{u}}^* = \widetilde{\boldsymbol{A}}^{-1}\boldsymbol{b}_{\boldsymbol{u}}$ using multigrid with initial guess $\boldsymbol{0}$.
2. Estimate pressure as $\boldsymbol{x}_p \approx -\widetilde{\mathcal{S}}^{-1}(\boldsymbol{D}\boldsymbol{x}_{\boldsymbol{u}}^* + \boldsymbol{b}_p)$.
3. Estimate velocity as $\boldsymbol{x}_{\boldsymbol{u}} \approx \widetilde{\boldsymbol{A}}^{-1}(\boldsymbol{b}_{\boldsymbol{u}} - \boldsymbol{G}\boldsymbol{x}_p)$ using a multigrid solver, starting with $\boldsymbol{x}_{\boldsymbol{u}}^*$ as an initial guess.

If exact solvers are employed the only approximation made in $\boldsymbol{P}_5$ is the approximation $\boldsymbol{S}^{-1} \approx \widetilde{\mathcal{S}}^{-1}$, and as such we expect it to be the best preconditioner in terms of the spectrum of the preconditioned operator. It is, however, also the most expensive of the five preconditioners because it involves two applications of $\widetilde{\boldsymbol{A}}^{-1}$. Our goal will be to investigate how well these preconditioners perform in practice with inexact subsolvers.

3. Numerical Implementation. In this section we specialize the relatively general preconditioners from the previous section to a specific second-order conservative finite-volume discretization of the time-dependent Stokes equations on a uniform rectangular grid. We do not discuss here the inclusion of advection in the full Navier-Stokes equations. Schemes that handle advection explicitly using a non-dissipative spatial discretization are described in detail in Refs. [40, 10].

3.1. Staggered-grid Discretization. For our numerical investigations of the various preconditioners we employ the well-known staggered-grid or MAC discretization of the Stokes equations [23, 22]. This is a conservative-discretization that is uniformly div-stable [38, 31]. The scheme defines the degree of freedoms at staggered locations. Specifically, scalar variables including pressure and density are defined at cell centers, while velocity components are defined at the corresponding faces of the grid. We illustrate this in two dimensions in Fig. 3.1 [**Donev: I suggest deleting this figure to reduce the length since everyone reading this will know this already**]; see Ref. [40] for additional details. In the figure, points marked by triangles are for the discrete velocity components $u \equiv u_x$ and $v \equiv u_y$, and points marked by circles correspond to the spatial location of the discrete density ρ, the viscosity μ, the bulk viscosity γ and the pressure p. For illustration, we assume that the domain Ω is rectangular and there are n_x cells along the x direction and n_y cells along the y direction, with periodic, no-slip (e.g., $\boldsymbol{u} = 0$ along a boundary) or free-slip (e.g., $v = 0$ and $du/dy = 0$ along the south boundary) boundary conditions specified at each of the domain boundaries. For simplicity, we further assume that the grid spacing along the different directions is constant, $h_x = h_y = h$.

agreed. Need to discuss how ρ enters system.

The divergence of $\boldsymbol{u} = (u, v)^T$ is approximated at cell centers by $\boldsymbol{D}\boldsymbol{u} = D^x u + D^y v$ with

$$(D^x u)_{i,j} = \frac{u_{i+1/2,j} - u_{i-1/2,j}}{h}, \qquad (D^y v)_{i,j} = \frac{v_{i,j+1/2} - v_{i,j-1/2}}{h}.$$

The gradient of p is approximated at the x and y edges of the grid cells (faces in three dimensions) by $\boldsymbol{G}p = (G^x p, G^y p)^T$ with

$$(G^x p)_{i-1/2,j} = \frac{p_{i,j} - p_{i-1,j}}{h}, \qquad (G^y p)_{i,j-1/2} = \frac{p_{i,j} - p_{i,j-1}}{h}.$$

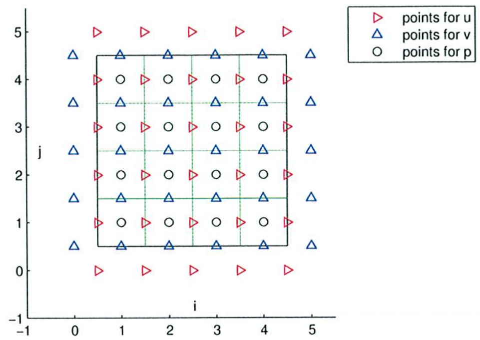

5 point (2D) / 7 point (3D)

FIG. 3.1. *A staggered-grid spatial discretization and the spatial location of the face-centered velocity and the cell-centered pressure degrees of freedom.*

For periodic domains or when a homogeneous Dirichlet condition is specified for the normal component of velocity at physical boundaries, the staggered discretization satisfies the co~~mpatibility (duality~~) $\boldsymbol{D} = -\boldsymbol{G}^*$. Note that $\boldsymbol{D}\boldsymbol{G} = \boldsymbol{L}_p$, where $\boldsymbol{L}_p$ is the standard $2d+1$ centered finite difference Laplacian.

For constant viscosity, the finite difference approximation to the vector Laplacian $\boldsymbol{\nabla}^2\boldsymbol{u}$ is denoted as $\boldsymbol{L}\boldsymbol{u} = (L^x u,\, L^y v)$. In the interior of the domain, $\boldsymbol{\nabla}^2 u$ is discretized using the standard five-point discrete Laplacian,

$$(L^x u)_{i-1/2,j} = \frac{u_{i+1/2,j} - 2u_{i-1/2,j} + u_{i-3/2,j}}{h^2} + \frac{u_{i-1/2,j+1} - 2u_{i-1/2,j} + u_{i-1/2,j-1}}{h^2},$$

and similarly for v. In the presence of physical boundaries, $L^x u$ is defined at all interior edges/faces where u are defined, and $L^y v$ is defined at all interior edges/faces where v are defined. The finite-difference stencils for tangential velocities next to no-slip and free-slip boundaries are modified to account for the boundary conditions, as described in Ref. [40]. Note that for constant viscosity, if one uses the Laplacian form of the viscous term, the different components of velocity are uncoupled.

When the viscosity is not a constant, the strain tensor form of the viscous term is needed. Note that

$$\boldsymbol{\tau}(\boldsymbol{u}) = \mu\left[\boldsymbol{\nabla}\boldsymbol{u} + (\boldsymbol{\nabla}\boldsymbol{u})^T\right] = \mu\begin{bmatrix} 2\frac{\partial u}{\partial x} & \frac{\partial u}{\partial y} + \frac{\partial v}{\partial x} \\ \frac{\partial u}{\partial y} + \frac{\partial v}{\partial x} & 2\frac{\partial v}{\partial y} \end{bmatrix},$$

how to average μ.

and therefore

$$\boldsymbol{L}_\mu \boldsymbol{u} = \boldsymbol{\nabla}\cdot\boldsymbol{\tau}(\boldsymbol{u}) = \begin{bmatrix} 2\frac{\partial}{\partial x}\left(\mu\frac{\partial u}{\partial x}\right) + \frac{\partial}{\partial y}\left(\mu\frac{\partial u}{\partial y} + \mu\frac{\partial v}{\partial x}\right) \\ 2\frac{\partial}{\partial y}\left(\mu\frac{\partial v}{\partial y}\right) + \frac{\partial}{\partial x}\left(\mu\frac{\partial v}{\partial x} + \mu\frac{\partial u}{\partial y}\right) \end{bmatrix}. \tag{3.1}$$

The discretization of $\boldsymbol{\nabla}\cdot\boldsymbol{\tau}(\boldsymbol{u})$ is constructed using standard centered second-order differences to give the discrete viscous operator $\boldsymbol{L}_\mu$. Note that even for constant viscosity, there is coupling between the velocity components in (3.1). For the staggered discretization that we employ here, it can be shown that for constant viscosity $\boldsymbol{L}_\mu\boldsymbol{u} = \mu\boldsymbol{L}\boldsymbol{u}$ if $\boldsymbol{D}\boldsymbol{u} = 0$. That is, the solution of the Stokes system is not affected by the choice of the form of the viscous term (this is to be contrasted with fractional step methods, where the unprojected velocity and therefore the projected velocity is affected by the choice). However, the Stokes solver is in general affected by the choice of the viscous term, even for constant viscosity.

[**Donev: For the sake of shortening the paper, I suggest we delete all of the stencils (3.2)-(3.7) – they are easy to construct and also given elsewhere.**] Explicitly, for the x-

component of momentum we discretize

$$\left[\frac{\partial}{\partial x}\left(\mu\frac{\partial u}{\partial x}\right)\right]_{i+1/2,j} = \frac{(\mu\frac{\partial u}{\partial x})_{i+1,j} - (\mu\frac{\partial u}{\partial x})_{i,j}}{h} \tag{3.2}$$

where

describe in words.

$$\left(\mu\frac{\partial u}{\partial x}\right)_{i,j} = \mu_{i,j}\left(\frac{u_{i+1/2,j} - u_{i-1/2,j}}{h}\right), \tag{3.3}$$

$\nabla\left(\beta-\frac{2}{3}\mu\right)\nabla u$

we discretize

$$\left[\frac{\partial}{\partial y}\left(\mu\frac{\partial u}{\partial y}\right)\right]_{i+1/2,j} = \frac{(\mu\frac{\partial u}{\partial y})_{i+1/2,j+1/2} - (\mu\frac{\partial u}{\partial y})_{i+1/2,j-1/2}}{h} \tag{3.4}$$

where

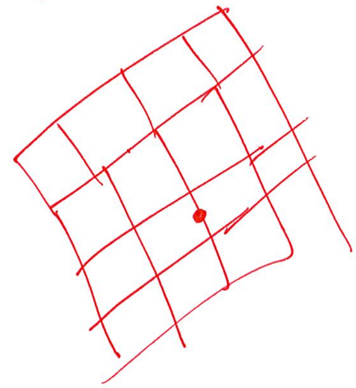

$$\left(\mu\frac{\partial u}{\partial y}\right)_{i+1/2,j+1/2} = \mu_{i+1/2,j+1/2}\left(\frac{u_{i+1/2,j+1} - u_{i+1/2,j}}{h}\right), \tag{3.5}$$

and we discretize

$$\left[\frac{\partial}{\partial y}\left(\mu\frac{\partial v}{\partial x}\right)\right]_{i+1/2,j} = \frac{(\mu\frac{\partial v}{\partial x})_{i+1/2,j+1/2} - (\mu\frac{\partial v}{\partial x})_{i+1/2,j-1/2}}{h} \tag{3.6}$$

where

$$\left(\mu\frac{\partial v}{\partial x}\right)_{i+1/2,j+1/2} = \mu_{i+1/2,j+1/2}\left(\frac{v_{i+1,j+1/2} - v_{i,j+1/2}}{h}\right). \tag{3.7}$$

The discretization for the y-component of momentum is identical, and bulk viscosity can be included straightforwardly. As described in Ref. [10], centered differences for the viscous fluxes that require values outside of the physical domain are replaced by one-sided differences that only use values from the interior cell bordering the boundary and boundary values. The tangential momentum flux is set to zero for any faces of the corresponding control volume that lie on a free-slip boundary, and values in cells outside of the physical domain are never required. The overall discretization is spatially globally second-order accurate.

We build the discrete velocity operator $\boldsymbol{A} = \theta\boldsymbol{\rho} - \boldsymbol{L}_{\boldsymbol{\mu}}$ from the above centered finite-difference operators. We assume that the density ρ is specified at the cell centers. The density matrix $\boldsymbol{\rho}$ is constructed by defining the discrete momentum density $\boldsymbol{\rho u}$ at the cell faces, where the corresponding velocity components are defined. Here we follow Ref. [10] and average the density from cell centers to cell faces,

$$(\boldsymbol{\rho u})_{i+1/2,j} = \left(\frac{\rho_{i,j}+\rho_{i+1,j}}{2}\right)u_{i+1/2,j} \quad \text{and} \quad (\boldsymbol{\rho u})_{i,j+1/2} = \left(\frac{\rho_{i,j}+\rho_{i,j+1}}{2}\right)v_{i,j+1/2},$$

giving a diagonal density matrix $\boldsymbol{\rho}$ with the interpolated face-centered densities along the diagonal. We will assume here that the shear $\boldsymbol{\mu}$ and bulk viscosities γ are specified at the cell centers; typically they are an explicit function of other scalar variables such as density, temperature and composition. The matrices $\boldsymbol{\mu}$ and γ that appear in the approximation to the Schur complement [e.g. Eq. (2.7)] are diagonal matrices containing the cell-centered values of the shear and bulk viscosities. The discretization of the viscous operator $\boldsymbol{L}_{\boldsymbol{\mu}}$ is defined by (3.2)-(3.7) and requires a shear viscosity at both cell-centers and nodes. The value of μ at a node is set to be the average of the four neighboring cell-centered values [10].